EnergyChem 4 (2022) 100076

Contents lists available at ScienceDirect

EnergyChem

journal homepage: www.sciencedirect.com/journal/energychem

Recent progress of artificial interfacial layers in aqueous Zn metal batteries

Peixun Xiong [a], Ye Zhang [b], Jingran Zhang [c], Sang Ha Baek [a], Lingxing Zeng [c], Yan Yao [b], Ho Seok Park [a,d,*]

[a] School of Chemical Engineering, Sungkyunkwan University, 2066 Seobu-ro, Jangan-gu, Suwon-si, Gyeonggi-do 16419, Republic of Korea
[b] Department of Electrical and Computer Engineering and Texas Center for Superconductivity, University of Houston, Houston, Texas 77204, United States
[c] Engineering Research Center of Polymer Green Recycling of Ministry of Education, College of Environmental Science and Engineering, Fujian Normal University, Shangsan Road No.8, Fuzhou, 350007, People's Republic of China
[d] SKKU Advanced Institute of Nanotechnology (SAINT), College of Engineering & Department of Health Sciences and Technology, Samsung Advanced Institute for Health Sciences and Technology (SAIHST), Sungkyunkwan University, Seobu-ro, Jangan-gu, Suwon-si, Gyeonggi-do 16419, Republic of Korea

ARTICLE INFO

Keywords:
Artificial interfacial layers
Zn metals
Aqueous batteries
Mechanism
ESS

ABSTRACT

Aqueous Zn metal batteries (AZBs) are considered as a promising candidate of existing lithium-ion batteries for grid-scale energy storage systems owing to their inherent safety, low cost, and natural abundance. However, the practical application of AZBs is still limited by severe dendrites, corrosion, and hydrogen evolution on zinc (Zn) anode as well as the dissolution of most cathode materials. Although Zn metals are relatively stable in mildly acidic aqueous electrolytes even without solid-electrolyte interphase (SEI), the interfacial structure becomes more significant in resolving the afore-mentioned problems. Herein, we comprehensively review the latest progress on the artificial interfacial layers (AILs) for high performance and safe AZBs. Addressing the fundamentals and challenges of AZBs, the functionality and design of AILs will be introduced discussing the current development of surface modified interphase, electrolyte derived SEI, and cathode/electrolyte interphase. Advanced characterization and simulation methods are also summarized for comprehensive analysis on failure and mechanism of AILs. Finally, our perspectives into future research direction of AILs will be presented.

1. Introduction

The transformation of the energy paradigm from current fossil fuels to renewable energies has driven the development of grid-scale energy storage system (ESS) for the realization of carbon neutrality and sustainable society[1–3]. Although rechargeable lithium-ion batteries (LIBs) are dominating the existing markets for portable electronics and electrical vehicles, it is very difficult to meet the requirements for ESS. In particular, LIBs are far from satisfactory for safety and cost: the organic electrolytes used in LIBs are flammable and toxic for safety concerns[4, 5] and the lithium resource is limited for high cost.[6, 7] In a sharp contrast to LIBs using organic electrolytes, aqueous batteries have the advantages in terms of high ionic conductivity, safety, and low cost (Fig. 1a).[8, 9] As shown in Fig. 1b, various metal batteries using metal anodes such as Na[10]., K[11]., Mg[12]., Ca[13]., Zn[14]., and Al[15]. have been intensively exploited to be free from safety and cost issues of LIBs while achieving the high specific capacity for a large energy density. Although aqueous metal batteries that configure non-Li metal anodes in aqueous electrolytes are expected to replace state-of-art LIBs for an application into ESS, thermodynamic constraint is not satisfied for most metal anodes that have incompatible plating/striping potentials with electrochemical stability window of aqueous electrolytes. Thermodynamically, aqueous electrolyte shows an electrochemical stability window of 1.23V, and the hydrogen evolution reaction (HER) potential is in the range of –0.83 to 0 V *vs.* SHE, depending on the pH value of electrolyte[16]. The redox potentials of Na/Na^+ (–2.71 V *vs.* SHE), K/K^+ (–2.92 V *vs.* SHE), Mg/Mg^{2+} (–2.36 V *vs.* SHE), Ca/Ca^{2+} (–2.86 V *vs.* SHE), and Al/Al^{3+} (–1.67 V *vs.* SHE) are lower than the potential of HER, suggesting that the corresponding metal anodes are thermodynamically unstable in aqueous electrolytes, and intrinsic HER occurs before metal plating in the process of electrochemical reduction.

Among these metal batteries, aqueous Zn metal batteries (AZBs) are particularly attractive owing to their high theoretical volumetric capacity (5851 mAh cm^{-3}, 2.8 times higher than that of Li), natural abundance in the Earth's crust (79 ppm, 4.6 times higher than that of Li), and proper redox potential (−0.76 V *vs.* SHE) within a narrow potential window of aqueous electrolyte as previously reviewed[17–29]. However, it is very difficult to avoid technical issues, including dendritic

* Corresponding author.
E-mail address: phs0727@skku.edu (H.S. Park).

https://doi.org/10.1016/j.enchem.2022.100076

Available online 6 June 2022

growth, corrosion, and hydrogen (H_2) release on the surface of Zn metal anodes in aqueous electrolytes[30]. Besides, most of high capacity cathode materials are attributed to a rapid capacity fading and short lifespan of the full batteries, which originates from structural collapse, dissolution, and side reactions in aqueous electrolytes[31–33]. Motivated by that these issues can be resolved controlling the interfacial structure and interaction, artificial interfacial layers (AILs) that play a similar role of the solid/electrolyte interphase (SEI) or cathode/electrolyte interphase (CEI) have been significantly investigated[34–40].

Considering the rapidly increasing academic and industrial interests on AZBs, we report a comprehensive and timely review on the latest progress of AILs focusing on three chemical approaches of surface modified interphase, electrolyte derived SEI, and CEI (Fig. 2). The fundamentals and technical challenges of Zn metal anodes and cathode materials in the mild acidic electrolytes will be discussed in Section 2. In Section 3, the functionality and design of AILs and their current development in AZBs will be addressed with a specific and in-depth discussion of the mechanisms. Advanced characterization and simulation methods are also introduced in Section 4. Finally, our perspectives and outlooks into a future direction of AILs for high performance and safe AZBs will be presented in Section 5.

2. Fundamentals and challenges in AZBs

Although AZBs, which employ Zn metal as the anode, Zn-intercalating materials as the cathode, and mildly acidic Zn-containing solution solutions as the electrolyte, have currently received significant attention as alternative battery system for ESS, the interphase issues between electrolyte and electrode greatly impede the large-scale deployment of AZBs[17–29]. In particular, the parasitic reactions in Zn anodes (corrosion, hydrogen evolution reaction (HER), and dendrite formation) and the absence of high-performance and compatible cathode materials are the major challenges towards AZBs.

Fig. 3a shows the schematic diagram of relative electron energies in the electrodes and aqueous electrolyte of a thermodynamically stable battery cell[41]. The chemical potentials of the cathode (μ_C) and anode (μ_A) should be ranged between the lowest unoccupied molecular orbital (LUMO) and the highest occupied molecular orbital (HOMO) of the aqueous electrolyte or within the energy separation E_g, corresponding to the electrochemically stable window. When the thermodynamic energy levels are well aligned, AZBs are spontaneously discharged and non-spontaneously charged in a galvanic and electrolytic mode, respectively, shuttling back and forth Zn ions of aqueous electrolytes between cathodes and anodes in a similar manner to "rocking-chair" working mechanism of LIBs. If not aligned properly, the electrolyte can be reduced on the anode side and/or oxidized on the cathode to produce H_2 and/or oxygen (O_2) gases, respectively, for a permanent cell failure. The noticeable difference between LIBs and AZBs is associated with the electrolyte solvent used and the corresponding interfacial chemistry. In LIBs, a mechanically robust, electrochemical inactive, ionically conducting, and electronically insulating SEI and/or CEI is formed from the decomposition of organic electrolytes, thereby suppressing the parasitic reaction between electrodes and electrolyte for a kinetically long-term stability of full batteries[42]. On the other hand, stable electrolyte/electrode interphase such as SEI or CEI in LIBs is absent in AZBs, which undesirable surface reaction on Zn anodes and cathodes is not

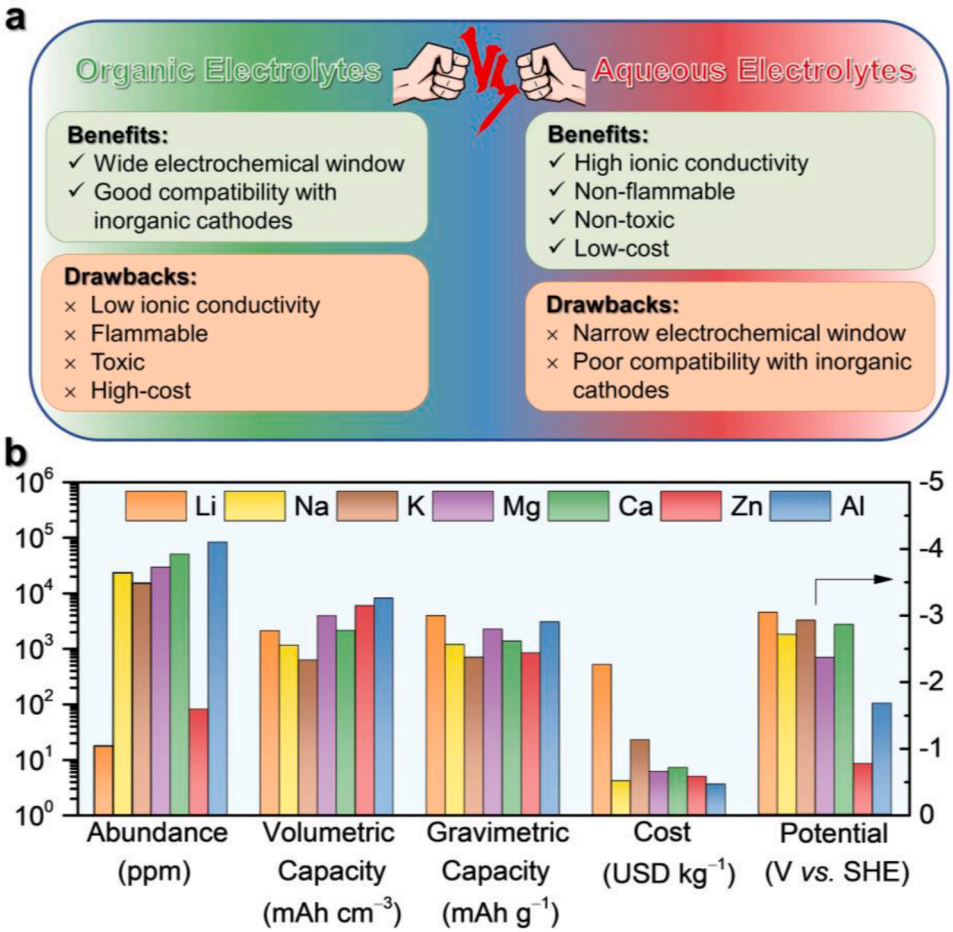

Fig. 1. (a) Comparison of the benefits and drawbacks between organic and aqueous electrolytes. (b) Abundance, specific capacity, cost, and standard electrode potentials of the representative metals. The price of metals is collected from the website of https://www.metal.com.

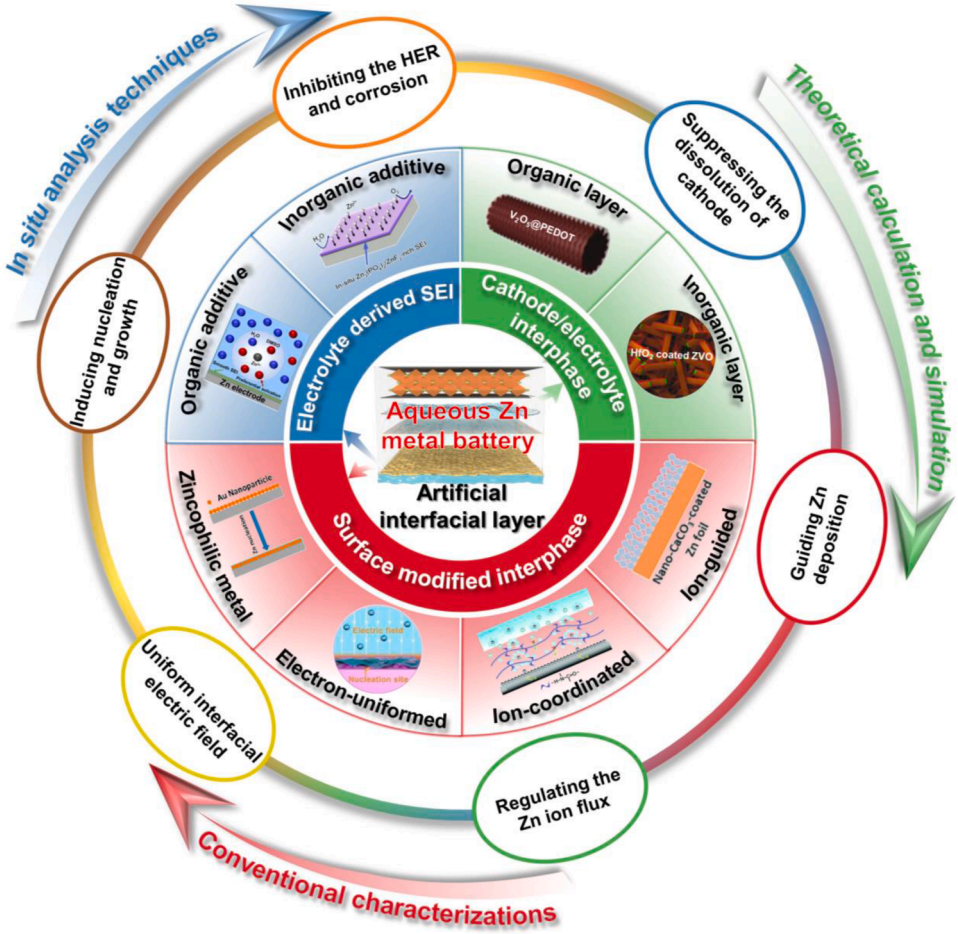

Fig. 2. Overview of artificial interfacial layers in aqueous Zn metal battery.

inhibited at the specific current densities and pH values but kinetically facile to a certain extent of what the battery performances are substantially undermined[43].

2.1. Corrosion and HER of Zn anodes

The Pourbaix diagram shows that the thermodynamically stable species within the electrochemical window of aqueous electrolyte are Zn^{2+}, ZnO, and $Zn(OH)_4^{2-}$ depending on the pH of electrolytes (Fig. 3b).[44, 45] Under alkaline conditions, metallic Zn reacts with OH^- to form zincate or $Zn(OH)_4^{2-}$ (Eq. 1). When $Zn(OH)_4^{2-}$ is locally saturated beyond the solubility limitation, this can be precipitated as ZnO on the anode surface (Eq. 2)[45–48].

$$Zn + 4OH^- \rightarrow Zn(OH)_4^{2-} + 2e^- \quad (1)$$

$$Zn(OH)_4^{2-} \rightarrow ZnO + H_2O + 2OH^- \quad (2)$$

Since these two-step reactions trigger the corrosion of Zn anode, where insulating ZnO passivates Zn surface for non-uniform Zn deposition, commercial alkaline Zn–air and Zn–MnO_2 batteries are not rechargeable or have a short cyclic lifespan. By contrast, the ZnO layer slows down the corrosion kinetics with a low self-discharge rate.[14, 49] Therefore, the optimization of the Zn/ZnO ratio is the key to design rechargeable alkaline Zn batteries[50].

Surface corrosion is alleviated at the mild acid conditions, whereas H_2 and OH^- can be released by the reaction of Zn metal with water (Eq. 3)[51].

$$Zn + 2H_2O \rightarrow Zn^{2+} + H_2\uparrow + 2OH^- \quad (3)$$

This reaction leads to the irreversible consumption of water, as well as changes the local pH to alkaline conditions. Consequently, insoluble $Zn(OH)_2$ or $Zn_4SO_4(OH)_6{\cdot}nH_2O$ is formed in $ZnSO_4$-containing electrolytes and precipitated as randomly packed sheets on the Zn surface, which increases the charge transfer resistance (Fig. 3c).[26, 51]

HER is also a critical consideration for the cell balance and safety of AZBs in mildly acidic aqueous electrolytes. Although HER is thermodynamically favorable owing to the higher potential of HER (0 V *vs.* SHE) than the redox potential of Zn/Zn^{2+} (−0.76 *vs.* SHE), the actual potential of HER can be lowered decreasing pH (−0.236 V at pH = 4) as determined by the Nernst Equation and the kinetics of HER can be sluggish during a Zn plating/striping process while increasing overpotential at high current densities.[52, 53] Nevertheless, HER, which can irreversibly consume Zn and water leading to the imbalanced N/P ratio and varied electrolyte formulation for the lowered Coulombic efficiency (CE) and capacity fading, as well as release H_2 gas for the increased inner pressure of a sealed cell, is often unavoidable at the given current rate and local pH[54].

2.2. Dendrite formation of Zn anode

Zn electrodeposition has been studied to regulate deposition morphologies. Zn electrodeposition behavior is based on diffusion-controlled growth mechanism in a similar manner to Li and Cu, in which metal dendrites would be formed if the current goes beyond the ion diffusion limit of the electrolytes (Fig. 4).[52, 55, 56] In most research works, the deposition current is typically below the transport limit of the electrolyte. The deposition morphology is affected by the competition between Zn deposition and SEI formation process[45]. At

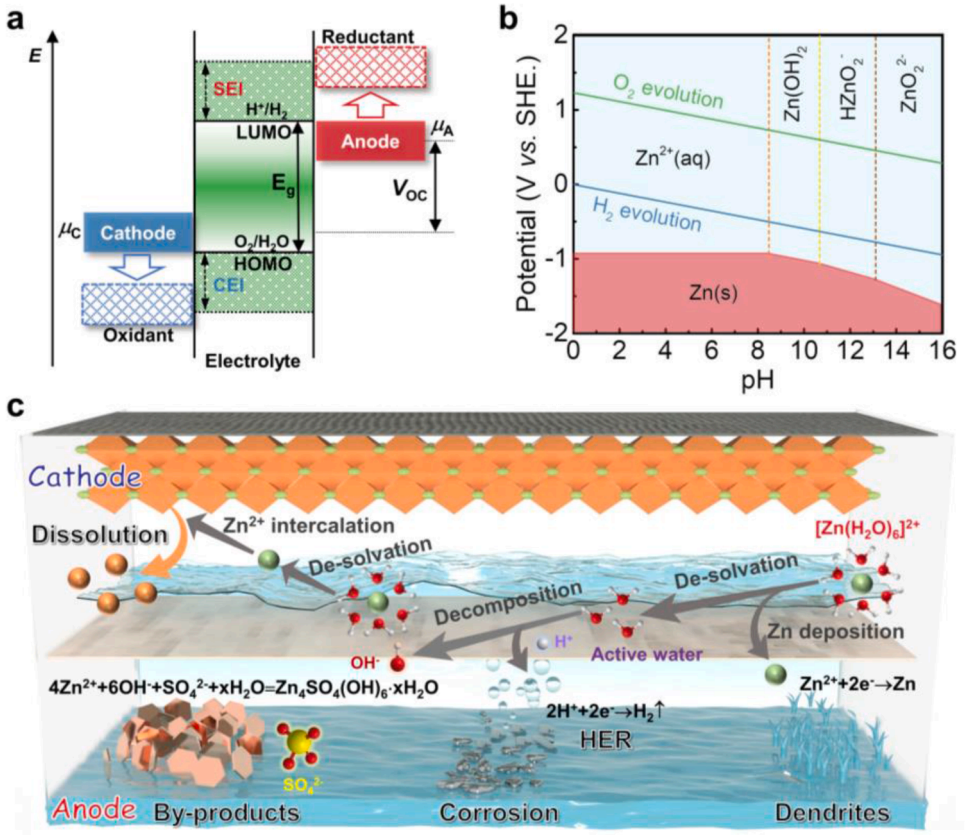

Fig. 3. (a) Schematic energy diagram of Zn anode and cathode in an aqueous electrolyte. (b) A Pourbaix diagram of Zn in an aqueous solution. (c) Technical challenges of Zn anode and cathode in $ZnSO_4$-containing electrolyte.

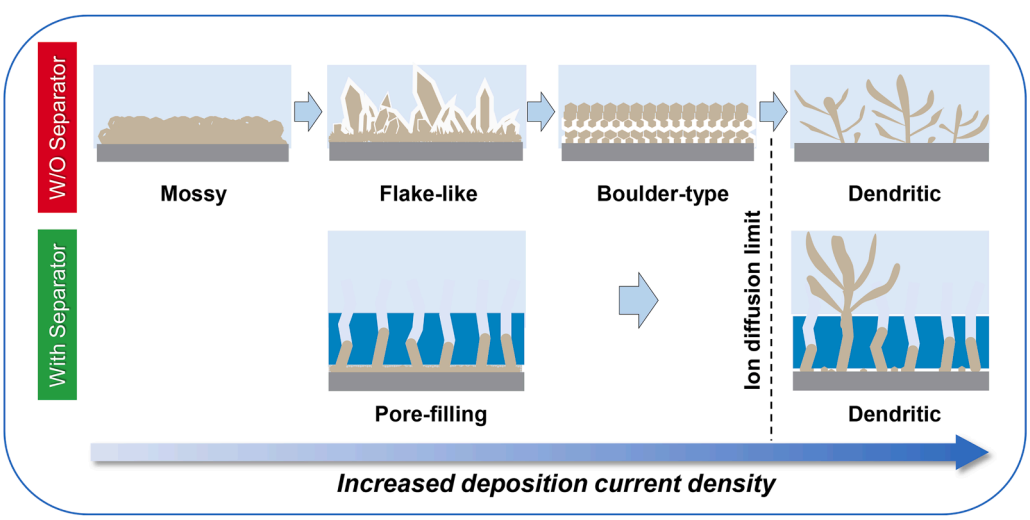

Fig. 4. Zn electrodeposition behaviors at different deposition current densities.

low current densities, mossy Zn can be grown as the SEI formation process dominates the surface reaction. Such morphology is commonly observed in alkaline conditions, where the surface reaction is prominent [57]. At moderate currents, Zn deposition dominates the reaction. The flake-like deposits are dominant because Zn preferentially exposes the (002) plane to minimize their surface energy[58]. These metal flakes with sharp tips and low packing density are often observed and unfavorable for the long cycle stability of AZBs.[59, 60] At high current densities, Zn can be deposited as relatively dense and uniform boulder-like layers, which result in suppressing the surface reactions. [56, 58, 60]

Previous studies about Zn electrodeposition are typically performed without separators or with separators peeled off. The presence of separators was found to strongly affect metal deposition morphologies[60]. For instance, the use of porous separators, like glass fiber or polypropylene, regulates Zn to be deposited onto their porous structures. Such pore-filling behavior is associated with the metal penetration of separators during the deposition process and trapping of unreacted dead Zn upon stripping. Using nonporous separators, dense and uniform Zn deposits can be formed underneath separators. These results elucidate

that, in addition to manipulating the intrinsic Zn deposition morphology, the microstructure of the separator is an indispensable factor to develop efficient AZBs.

2.3. Development of advanced cathode materials

Various inorganic compounds, such as Mn-based, V-based, and Prussian blue analog-based materials, have been investigated as cathodes of AZBs as previously reviewed.[17, 18, 61] These materials are typically featured with a layered or open tunnel structure to accommodate divalent Zn^{2+} accompanied by H^+ co-insertion[62–64]. While the participation of H^+ enhances the kinetics of cathode reactions, local pH values are changed to the alkaline condition through the formation of hydroxide compounds resulting in the surface passivation of Zn anode. Although the formation of these compounds is reversible at a low loading mass of active material,[63, 64] this becomes problematic with the thick electrode because the insulating hydroxide compounds deteriorate electron conduction in the cathode[65]. Recently, some organic compounds have been developed as low-cost, environmentally friendly cathode materials for AZBs[66]. Unlike the charge storage of inorganic cathodes *via* Zn^{2+} diffusion into the intercalation host, organic materials store charges through the coordination reactions, which bypasses the slow solid-state diffusion. Furthermore, the charge storage of some organic molecules and polymers is independent of proton participation [67–69]. The comparison of all kinds of advanced cathode materials (Mn-based compounds, V-based compounds, Prussian blue analogues, polyanionic compounds, metal sulfides, and organic compounds) based on their specific capacity and discharge voltage plateau are summarized in Table 1.[62–64, 70–91] Although most of cathodes exhibited a high capacity retention over thousands of cycles, their average discharge voltages were still less than 2.0 V which is lower than the commercialized LIBs (>3.5 V). Hence, developing advanced cathode materials with long cycle life and high discharge voltage is crucial to achieve high-energy-density AZBs[29].

Table 1
Comparison of electrochemical performances of all kinds of advanced cathode materials.

Type	Electrode	Electrolyte	Voltage window @average discharge voltage (V *vs.* Zn/Zn^{2+})	Specific capacity (mAh g^{-1})	Capacity retention @cycles@current density	Refs.
Mn-based compounds (1C=308 mA h g^{-1})	α-MnO_2	2M $ZnSO_4$ + 0.1M $MnSO_4$	1.0–1.9 @~1.30	285@C/3	92%@5000@5C	63
	β-MnO_2	3M $Zn(CF_3SO_3)_2$ + 0.1M $Mn(CF_3SO_3)_2$	0.8–1.9 @~1.35	258@0.65C	94%@2000@6.5C	70
	γ-MnO_2	1M $ZnSO_4$	0.8–1.8 @~1.30	285@0.05 mA cm-2	63%@40@0.05 mA cm-2	71
	δ-MnO_2	1M $Zn(TFSI)_2$ + 0.1M $Mn(TFSI)_2$	1.0–1.8 @~1.30	238@0.2C	93%@4000@20C	64
	ε-MnO_2	2M $ZnSO_4$ + 0.2M $MnSO_4$	1.0–1.8 @~1.30	290 at 0.3C	~100%@10000@6.5C	62
	$ZnMn_2O_4$	3M $Zn(CF_3SO_3)_2$	0.8–1.9 @~1.35	150 mA h g^{-1} at 50 mA g^{-1}	94%@500@500 mA g^{-1}	72
V-based compounds	$Zn_{0.25}V_2O_5{\cdot}nH_2O$	1M $ZnSO_4$	0.5–1.4 @~0.81	282 mA h g^{-1} at 300 mA g^{-1}	80%@1000@2400 mA g^{-1}	73
	VO_2	1M $ZnSO_4$	0.2–1.2 @~0.50	326 mA h g^{-1} at 50 mA g^{-1}	86%@5000@3000 mA g^{-1}	74
	V_2O_5	3M $Zn(CF_3SO_3)_2$	0.2–1.6 @~0.72	470 mA h g^{-1} at 0.2 A g^{-1}	91.1%@4000@5 A g^{-1}	75
	V_6O_{13}	1M $Zn(CF_3SO_3)_2$	0.2–1.5 @~0.70	360 mA h g^{-1} at 200 mA g^{-1}	92%@2000@4 A g^{-1}	76
	$Na_2V_6O_{16}{\cdot}1.63H_2O$	3M $Zn(CF_3SO_3)_2$	0.2–1.6 @~0.70	352 mA h g^{-1} at 50 mA g^{-1}	90%@6000@5 A g^{-1}	77
Prussian blue analogues	ZnHCF	1M $ZnSO_4$	0.8–1.9 @~1.70	65.4 mA h g^{-1} at 60 mA g^{-1}	81%@100@300 mA g^{-1}	78
	NiHCF	0.5M Na_2SO_4 + 0.05M $ZnSO_4$	0.9–1.9 @~1.50	76.2 mA h g^{-1} at 100 mA g^{-1}	81%@1000@500 mA g^{-1}	79
	ZnHCF@MnO_2	0.5M $ZnSO_4$	1.4–1.9 @~1.70	118 mA h g^{-1} at 100 mA g^{-1}	77%@1000@500 mA g^{-1}	80
	CoHCF	4M $Zn(CF_3SO_3)_2$	0.7–2.0 @~1.75	173 mA h g^{-1} at 0.3 A g^{-1}	100%@2200@3 A g^{-1}	81
Polyanionic compounds	$Na_3V_2(PO_4)_3$	0.5M $Zn(CH_3COO)_2$	0.8–1.7 @~1.10	97 mA h g^{-1} at 0.5C	74%@100@50 mA g^{-1}	82
	$Na_3V_2(PO_4)_2F_3$/C	2M $Zn(CF_3SO_3)_2$	0.8–1.9 @~1.62	75 mA h g^{-1} at 80 mA g^{-1}	95%@4000@1000 mA g^{-1}	83
	$Na_3V_2(PO_4)_3$/rGO	2M $Zn(CF_3SO_3)_2$	0.6–1.8 @~1.23	114 mA h g^{-1} at 50 mA g^{-1}	75%@200@500 mA g^{-1}	84
Metal sulfides	VS_2	1M $ZnSO_4$	0.4–1.0 @~0.62	190 mA h g^{-1} at 50 mA g^{-1}	99%@200@500 mA g^{-1}	85
	MoS_2	1M $ZnSO_4$	0.2–1.6 @~0.60	203 mA h g^{-1} at 100 mA g^{-1}	98.6%@600@1 A g^{-1}	86
	VS_4	1M $ZnSO_4$	0.4–1.0 @~0.80	310 mA h g^{-1} at 100 mA g^{-1}	85%@500@2.5 A g-1	87
Organic compounds	Calix quinone	3M $Zn(CF_3SO_3)_2$	0.8–1.3 @~1.0	335 mA h g^{-1} at 20 mA g^{-1}	87%@1000@500 mA g^{-1}	88
	PQ-Δ	3M $Zn(CF_3SO_3)_2$	0.25–1.6 @~0.78	225 mA h g^{-1} at 30 mA g^{-1}	99.9%@500@150 mA g^{-1}	89
	PANI	1M $Zn(CF_3SO_3)_2$	0.5–1.5 @~1.1	200 mA h g^{-1} at 50 mA g^{-1}	92%@3000@5 A g^{-1}	90
	DTT	2M $ZnSO_4$	0.3–1.4 @~0.75	209 mA h g^{-1} at 50 mA g^{-1}	83.8%@23000@2 A g^{-1}	91

3. State-of-the-art development of AILs in AZBs

3.1. Design and functionality of AILs

Although various cathode materials have been developed for AZBs, several fundamental issues regarding metal anodes still impede their commercialization[14]. The anode issues originate from the thermodynamic instability of Zn metals in aqueous electrolytes, which causes surface passivation and corrosion. Accordingly, the active sites for metal deposition are decreased. The localized metal deposition leads to the formation of loosely packed metal deposits with high aspect ratios, which not only penetrate the separator to short-circuit the cell, but also lead to a low stripping efficiency by detaching from the substrate. These deposits with high surface area will further boost the surface reactions, deteriorating anode performance and CE. An effective way to resolve the above-mentioned issues is to construct the well-designed AILs for the suppressed surface reactions. For example, surface coating or SEI formation strategies prevent direct contact between metal and water, preserving abundant active sites for homogenous metal deposition. Consequently, uncontrolled metal deposition is inhibited to form the uniform and dense deposition layers, which results in the long cycle stability and high efficiency of metal anode.

The decomposition products from water, *i.e.*, H_2 and hydroxide at anode or O_2 and H^+ at cathode, can be deposited in a solid state onto the electrode surfaces creating a protective interphase, because the plating/stripping of Zn in aqueous electrolytes is highly reactive and extremely unstable[92]. The emerging strategies into the construction of robust and functional AILs have been developed to stabilize the SEIs and CEIs, thus will be discussed in detail in the Sections 3.2 and 3.3.

3.2. AILs for Zn metal anode

The design of AILs is an effective way to regulate Zn deposition for uniform nucleation and flat deposition, which improves the interface stability and cycle lifetime of the Zn anode. This Section categorizes two types of AILs for Zn anode into surface modified interphase and functional electrolyte derived AILs along with the developmental timeline summarized in Fig. 5. The strategies for constructing surface modified are particularly classified into four types, including ion-guided layers, ion-coordinated layers, electron uniformed layers, and zincophilic metal layers. This Section will focus on the mechanisms and chemistries of these strategies.

3.2.1. Surface-modified AILs

3.2.1.1. Ion-guided layers. Ion-guided layers could construct Zn ion channels to homogenize the transfer of Zn ions. For example, Zhi *et al.* reported a simple and cost-effective porous $CaCO_3$ coating used as a buffer layer to ensure uniform and position-selected plating of Zn metal (Fig. 6a)[93]. The Zn plating reaction was confined to the surface region of Zn foils by porous coatings, which guided uniform electrolyte flux and Zn plating rate over the entire Zn foil surface, for a uniform, bottom-up Zn plating process. However, Zn deposits contact the electrolyte due to the porous characteristics of $CaCO_3$ coating layer, thus leading to corrosion and HER issues. Hence, other dense artificial layers were proposed to decorate the surface of Zn anode. For instance, Mai *et al.* coated a thin TiO_2 onto Zn metal *via* atomic layer deposition (ALD) method, which serves as a stable passivation layer for Zn metal, avoiding the direct contact between the Zn plate and electrolyte and suppressing Zn corrosion process and HER (Fig. 6b)[94]. The interactions between Zn and different facets of TiO_2 have been systematically investigated and found that (001) faceted TiO_2 protective layer had relatively low Zn affinity, which restrict dendrite formation and homogenize Zn deposition (Fig. 6c)[95]. However, the drastic volume change of Zn anode leads to the interfacial instability in the charge/discharge process. The TiO_2 composite with anti-corrosion elastic constraint and highly self-adaptable polymers could dynamically adapt to volume changes and inhibit dendrites growth, achieving highly reversible and long-life Zn|Zn symmetric cell performance at high current densities (> 10 mA cm^{-2}). [96, 97]

Other oxide compounds, such as ZnO,[98, 99] Al_2O_3,[100]. and $ZnMoO_4$[101]. were coated on the Zn surface to improve the plating/stripping efficiency. Xie *et al.* developed a 3D porous ZnO coating to accelerate the kinetics of Zn^{2+} transfer *via* the electrostatic attraction toward Zn^{2+} in electric double layers and to suppress the HER reaction (Fig. 6d)[98]. Consequently, 99.55% of Zn utilization and long-time stability for 1000 cycles were achieved. While the micron-sized ZnO coating layer results in increased interfacial resistance, leading to high

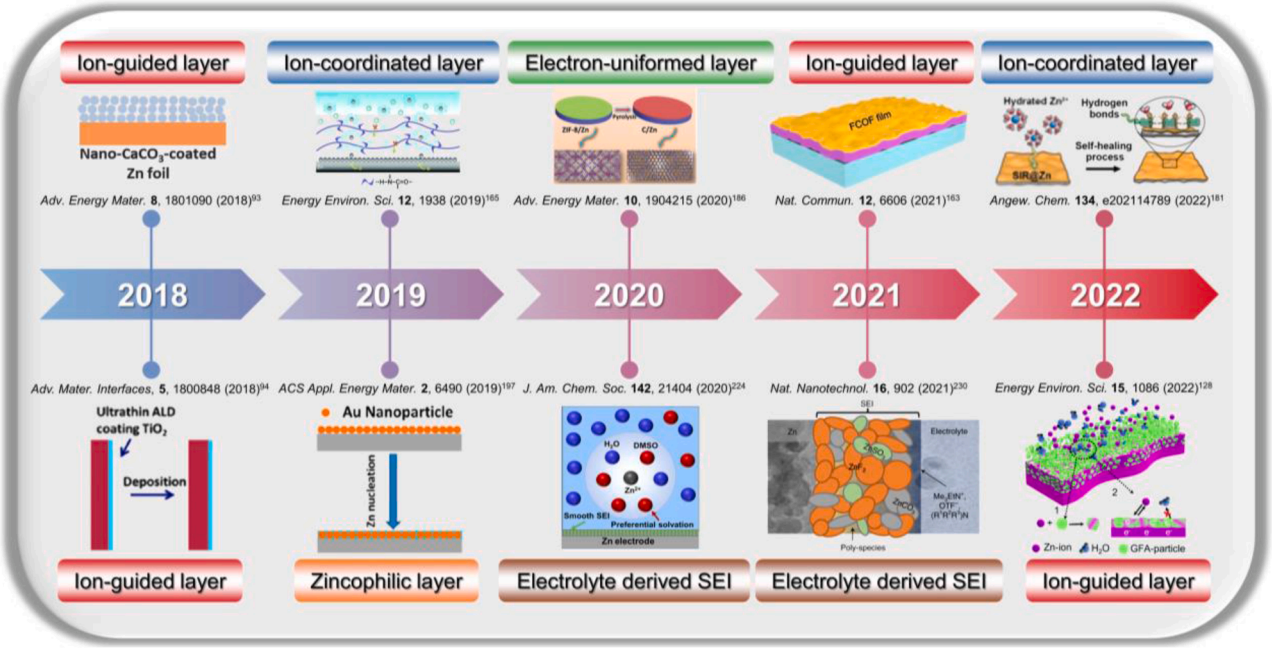

Fig. 5. Timeline of AILs for Zn anode from 2018 to 2022.

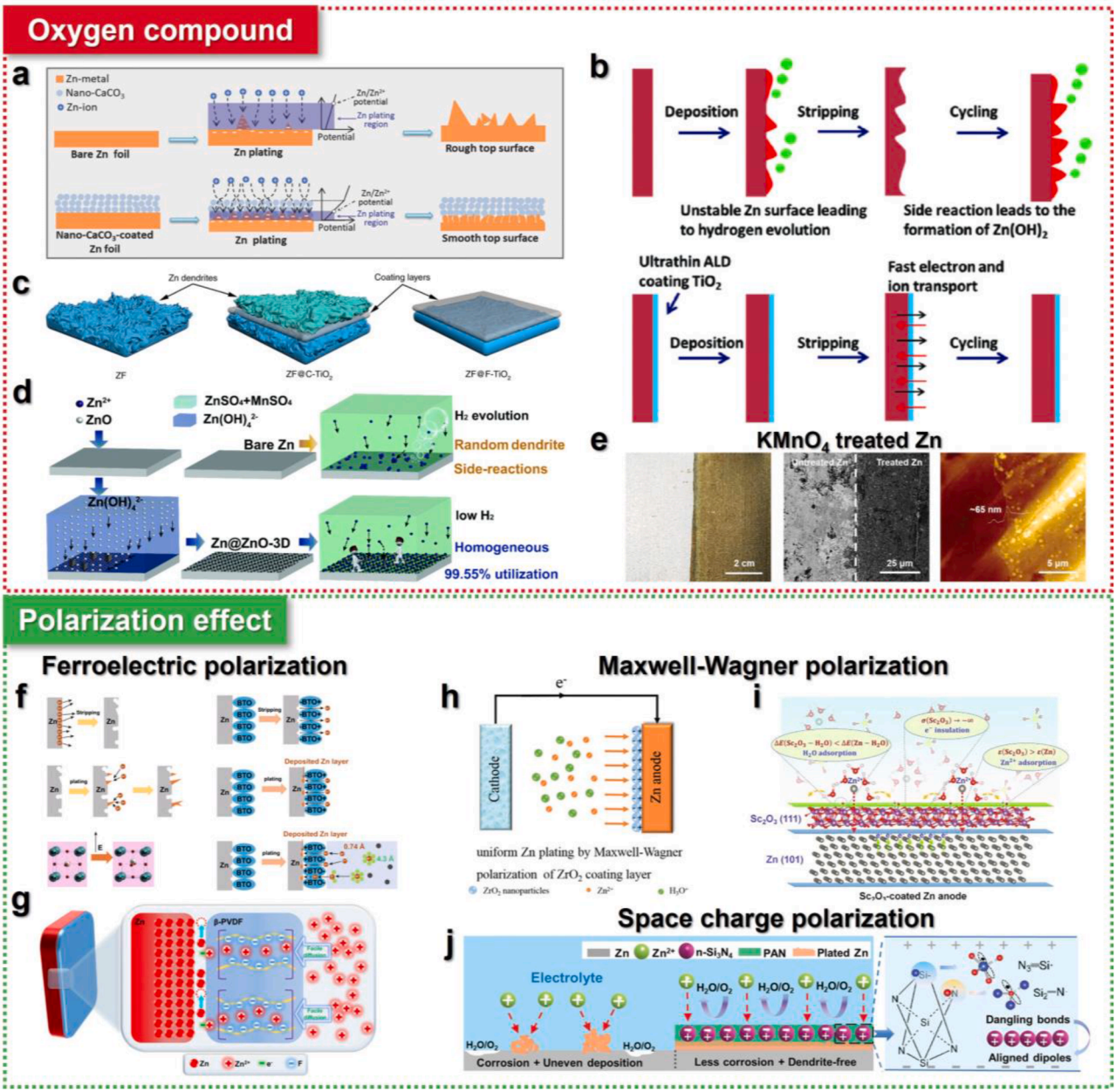

Fig. 6. (a) Schematic illustrations of morphology evolution for bare and nano-$CaCO_3$-coated Zn foils during Zn stripping/plating cycling. Reproduced with permission[93]. Copyright 2018, Wiley-VCH. (b) Schematic illustration of the stabilization of Zn anode without/with TiO_2 coating. Reproduced with permission[94]. Copyright 2018, Wiley-VCH. (c) Schematic illustration of the Zn plating process with different coating layers. Reproduced with permission[95]. Copyright 2020, Springer Nature. (d) Schematic images depicting the preparation Zn@ZnO-3D anode and deposition process in an aqueous electrolyte compared with bare Zn. Reproduced with permission[98]. Copyright, 2020 Royal Society of Chemistry. (e) Digital photo, SEM, and AFM images of untreated and treated areas on a foil. Reproduced with permission[102]. Copyright 2022, Wiley-VCH. (f) Schematic of Zn ion transport during Zn stripping/plating for bare Zn (left) and BTO@Zn foil (right). Reproduced with permission[103]. Copyright 2021, Springer. (g) Illustration of the ion distribution and uniform deposition through the β-PVDF membrane. Reproduced with permission[106]. Copyright, 2021 Elsevier. (h) Schematic the stripping/plating process of the ZrO_2-coated Zn anode. Reproduced with permission [108]. Copyright 2020, Wiley-VCH. (i) The schematic diagram of reaction process on the surface of Sc_2O_3-coated Zn anode. Reproduced with permission[109]. Copyright 2021, Elsevier. (j) Schematic illustration of Zn plating/stripping behavior on bare Zn (left panel) and Zn with PSN coating (middle panel). The right panel shows the amorphous Si_3N_4 nanoparticles exhibit novel dielectric behavior. Reproduced with permission[112]. Copyright 2021, Wiley-VCH.

overpotential, a periodic anodizing technique was developed to obtain a composite Zn anode comprising a Zn hexagonal pyramid array (HPA) coated with a functionalized ZnO layer (Zn@ZnO HPA), thus decreasing the local current density by means of the increased electroactive surface area of Zn anode[99]. More recently, an amorphous ZnMn-oxyhydroxide layer was constructed on the Zn surface *via* a rapid chemical treatment with $KMnO_4$ solution (Fig. 6e)[102]. The continuous, conformal, and robust protective layer on Zn surface is attributed to a uniform Zn plating/stripping and increased corrosion resistance, tolerating to manufacturing and processing defects on Zn metals.

Controlling the interfacial electric field was also demonstrated to make the charge distribution at the interphase more uniform. Recently, ferroelectric materials, such as $BaTiO_3$, [103, 104] $KTa_{0.54}Nb_{0.46}O_3$, [105]. polyvinylidene fluoride (PVDF),[106]. and poly(vinylidene fluoride-trifluoroethylene) (P(VDF-TrFE))[107]. have been employed to regulate Zn metal deposition as artificial interfacial layers (Fig. 6f-6g).

These materials could induce uniform and switchable electric polarization on their surface to guide ion migration. During the polarization changing process, the ferroelectricity can dynamically accelerate ion transport and homogenize ion flux by creating an internal electric field, thus achieving uniform and lateral deposition. To modify the interphase between the Zn anode and the electrolyte, Maxwell-Wagner polarization mechanism was proposed. Because of the large difference in dielectric constant (ε) and electrical conductivity (σ) between Zn anode and the coating layers (such as ZrO_2,[108]. Sc_2O_3,[109]. and CeO_2[110, 111]), a charge separation over a considerable distance will be formed at the interphase, which provides more nucleation sites and guarantees the uniform Zn stripping/plating (Fig. 6h-6i). Furthermore, silicon nitride (Si_3N_4) with abundant dangling bonds (e.g., $N_3{\equiv}Si$, $Si_2{=}N$, etc.) can confine a large amount of space charge (Fig. 6j)[112]. Under an external electric field, dipole moments can be aligned with specific orientations, which could guide the ion distribution/migration in the electrolyte and facilitate the uniform Zn electrodeposition. Besides, the insulating functional layers also have good chemical stability and increase hydrogen evolution overpotential that can suppress HER and inhibit other side reactions.

Although the above-mentioned external interfacial coating layers exhibit a certain mechanical strength to inhibit the growth of Zn dendrites and suppress the interfacial side reactions, they do not conduct Zn^{2+}, which may impede ion migration and have little effect to chemically modulate the interfacial Zn^{2+} flux. Inspired by the mature application of phosphates as metal protectors on large Equipment, a fast ion conductor of $NaTi_2(PO_4)_3$ with 3D porous nanoparticle structure and low electrochemical activity was employed as a solid-state electrolyte protection layer to induce uniform deposition of Zn^{2+} and inhibit interfacial side reactions (Fig. 7a)[113]. Therefore, stabilized Zn anode with high-rate performance and super long cycling life was realized in symmetrical cells and Zn/MnO_2 battery. Another kind of phosphates ($Zn_3(PO_4)_2$) featuring highly Zn^{2+} conductive was also reported to composite with Nafion, thus forming an organic-inorganic dual protection layer to stabilize the Zn anode (Fig. 7b)[114]. This synergistic protection layer can not only effectively suppress anion and free water molecule to react with Zn metal, but also enhances the Zn ionic conductivity which results in ultralow overpotential of Zn deposition/dissolution. Zhai *et al.* also used the Zn-ion interactable $V_2O_5{\cdot}nH_2O$ (VO) as the interfacial modifier to build a Zn^{2+}-conductive $Zn_xV_2O_5{\cdot}nH_2O$ (ZnVO) interfacial layer *via* the spontaneous chemical reaction between the pre-fabricated VO film and Zn metal foil[115]. The obtained ZnVO-coated Zn anodes can deliver 10 times longer cycle life with a dendrite-free morphology, reduced voltage polarization and high CE over 99% after 1000 cycles.

Introducing appropriate elements to form a coating layer (e.g., oxygen element) can also significantly modify the charge distribution of Zn surface and attain an unbalanced charge distribution at the Zn matrix-coating interphase to drive a faster Zn^{2+} diffusion during cycling. Hence, other non-oxygen elements, such as sulfur (S), selenium (Se), phosphorus (P), and fluorine (F), are doped into Zn lattice to form ZnS, [116, 117] ZnSe,[118–121]. ZnP,[122]. and ZnF_2[123–125]. as protective layers, respectively. In this case, an *in-situ* vapor–solid technique was used to build a compact artificial ZnS layer on the Zn metal surface, which might improve the reversibility of Zn metal due to the strong adhesion, mechanical strength, and high ionic conductivity of ZnS (Fig. 7c)[116]. Inspired by the results, Hou and Sun *et al.* successionally reported the utilization of ZnSe protective layer to stabilize Zn anode. [118, 119] The low Zn affinity of ZnSe and the unbalanced charge distribution at the interface can promote a uniform distribution of Zn^{2+} and accelerate Zn^{2+} migration, thus eliminating dendrite[118]. ZnSe coating serves as a cultivator to guide oriented growth of Zn (002) plane at the infancy stage of stripping/plating cycles, thereby inhibiting the formation of Zn dendrites and suppressing side reactions[119]. Furthermore, mixed conducting frameworks composed of electronic conductive MXene and ionic conductive ZnS/ZnSe layers were adopted to act as artificial layers for Zn anode with synergistic benefits.[117, 121] The 3D MXene can effectively guide Zn electrodeposition by homogenizing the distribution of electric field, decreasing local current density, and alleviating volume change. The ZnS can promote uniform Zn^{2+} distribution, accelerate Zn^{2+} migration, and inhibit side reactions. In addition, the ZnP alloy coated Zn foil was prepared *via* a high-efficiency electrodeposition method to achieve fast charging and high areal capacity[122]. The P atoms in the coating layer are beneficial to facilitating ion transfer and reducing the electrochemical activation energy during Zn stripping/plating processes. Besides, a lower energy barrier of Zn^{2+} transferring into the coating can be attained due to the additional P.

Inspired by the great progress of LiF-based SEI in Li metal anodes, ZnF_2 was developed to act as robust artificial SEI for Zn metal anode. Recently, Li *et al.* designed a 3D interconnected ZnF_2 matrix on the surface of Zn foil through a simple and fast anodic growth method, serving as a multifunctional protective layer, which not only redistributes the Zn^{2+} flux, but also reduces the desolvation active energy significantly, leading to stable and facile Zn deposition kinetics (Fig. 7d)[123]. At the same time, Zhi *et al.* constructed an electronically insulating (0.11 mS cm^{-1}) but highly Zn^{2+} conductive (80.2 mS cm^{-1}) ZnF_2 solid ion conductor with a high Zn^{2+} transfer number (0.65) to isolate Zn metal from the aqueous electrolyte, thus inhibiting side reaction and enhancing electrochemical reversibility of Zn metal electrode[124]. Latterly, Han *et al.* produced an artificial ZnF_2 layer for Zn anode with a thickness of 1 μm[125]. Their results suggest that ZnF_2 can allow insertion of Zn^{2+} and offers diffusion channels for the transport to/from the Zn anode *via* an interstitial diffusion mechanism that is different from the vacant mechanism. In addition, a 3D stacked lamellar matrix composed of $ZnF_2/Zn_3(PO_4)_2/CF_X$ was deposited onto Zn anode surface *via* thermal calcination and electrodeposition, delivering enhanced thermodynamic stability and rapid Zn^{2+} transport kinetics[126]. Very recently, artificially coating adopted by complexing zincophilic metal (such as Ag and Cu) with hydrophilic ZnF_2 was achieved through spontaneous displacement reactions. The hybrid ZnF_2-Ag surface are well-separated to promote the desolvation and nucleation processes simultaneously[127]. More importantly, a spatial gradient structure fluorinated alloy (GFA) with ZnF_2 at the outmost region and the CuZn alloy on the inside was constructed to enable a highly reversible Zn anode (Fig. 7e)[128]. It could accommodate a dendrite-free morphology by inducing lateral growth inside the GFA-coating layer based on two pathways: storing plated Zn by forming CuZn alloy inside the CuZn particles and filling the voids between the GFA particles. The zincophilic mechanism of metal elements will be discussed in greater detail in **3.2.1.4**. In addition, the gradient design was also accomplished in a Zn-doped MgF_2-based artificial layer by a radio frequency sputtering technique[129]. Consequently, the Zn-doped MgF_2 region is associated with fast Zn^{2+} transfer kinetics due to the interfacial polarization between the Zn dopant and the MgF_2 layer based on the Maxwell–Wagner effect, as well as the uniform deposition of Zn ions.

A uniform Zn metal nucleation also plays a crucial role to boost dendrite-free Zn anode. A strategy of introducing zincophilic sites shows promise in suppressing dendrite growth. Qiao *et al.* reported the mechanism of zincophilic sites based on employing multi *in situ/ex situ* techniques (Fig. 7f)[130]. By using a carbon-host as a model system with nitrogen sites as zincophilic sites, Zn ions are bonded with pyridine sites to form Zn–N bonds, inducing spacious nucleation of Zn on carbon-hosts and suppressing Zn-dendrite formation. In the early time, a zincophilic interphase based on 3D-printed graphite-C_3N_4 modulating interface with the uniform nucleating electron field (the rich N species) and fast electron transport (3D porous structure and innately rich structural defects) was constructed to achieve the formation of strong Zn–N transient states to capture Zn^{2+}, which induce the stabilization and uniformity of Zn distribution to further control the dendrite growth[131]. Recently, boron nitride (BN) with excellent mechanical robustness and chemically inert has been applied as interfacial layers on Zn anode.[132, 133] The rich Lewis acid sites (B atoms) and zincophilic sites (N atoms)

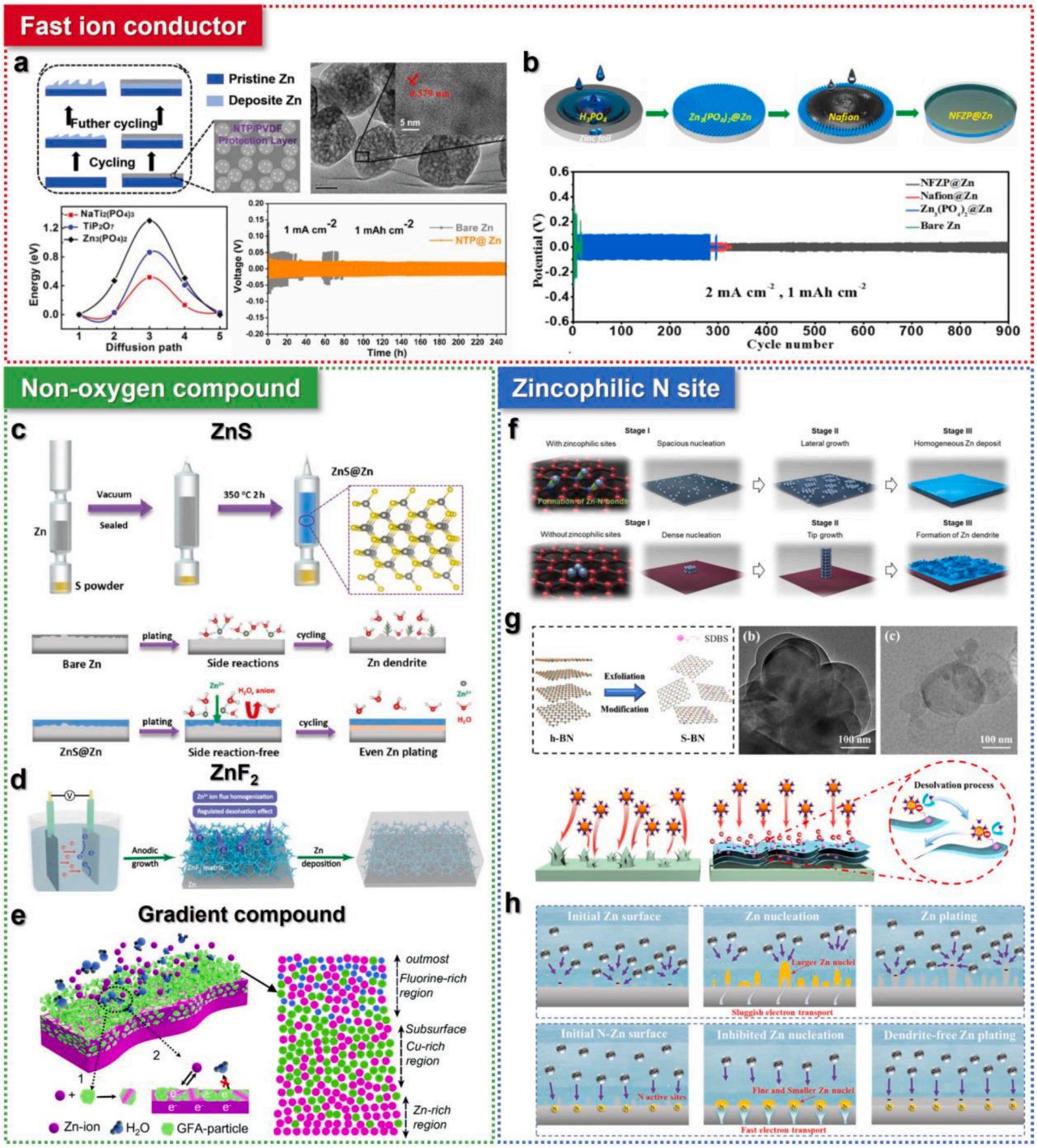

Fig. 7. (a) Upper: schematic illustration of the stabilization of NTP@Zn; lower left: proposed migration energy barriers of Zn ion in bulk NTP, TPO, and ZPO; lower right: long-term galvanostatic cycling of symmetrical Zn cells with NTP@Zn foil and bare Zn foil at a current density of 1 mA cm^{-2}. Reproduced with permission[113]. Copyright 2020, Wiley-VCH. (b) Upper: schematic illustration of the fabrication process of the NFZP@Zn electrode; lower: polarization voltage of NFZP@Zn, Nafion@Zn, $Zn_3(PO_4)_2$@Zn and bare Zn symmetrical cells with a current density of 2 mA cm^{-2}. Reproduced with permission[114]. Copyright 2022, Elsevier. (c) Upper: introducing the ZnS layer on the surface of Zn metal substrate by an *in situ* strategy; lower: schematic illustration of the artificial ZnS layer and Zn plating behavior with/without ZnS. Reproduced with permission[116]. Copyright 2020, Wiley-VCH. (d) Schematic illustration of the fabrication of the Zn@ZnF_2 electrode. Reproduced with permission[123]. Copyright 2021, Wiley-VCH. (e) Left: schematic of Zn-ion transfer and the electron flow pathway during the Zn deposition process on GFA-5, where the 1st step is the alloying process, and the 2nd is the filling of the voids; right: illustration of the elemental distribution inside a GFA particle. Reproduced with permission[128]. Copyright 2022, Royal Society of Chemistry. (f) Upper: spacious Zn nucleation and homogeneous Zn deposition on surface with zincophilic sites; lower: dense nucleation and subsEquent formation of Zn-dendrite on zincophobic surface. Reproduced with permission[130]. Copyright 2021, Wiley-VCH. (g) Upper left: schematic illustration for the S-BN nanosheet preparation process; upper right: TEM images of h-BN and S-BN; lower: Proposed mechanism for the Zn plating behavior of bare Zn and S-BN@Zn electrodes. Reproduced with permission.[133]. Copyright 2022, Elsevier. (h) Proposed mechanism for different Zn nucleation and plating behaviors of Zn and N-Zn electrodes. Reproduced with permission[134]. Copyright 2021, Wiley-VCH.

of the BN interface could greatly affect the Zn^{2+} concentration gradient and internal electric field on Zn surface[132]. Given by neither permanent charges nor movable cations in the BN structure, modification of BN with sulfonate group (S-BN) could promote the favorable desolvation process of hydrated Zn ions and improve the Zn ion migration rate (Fig. 7g)[133]. A facile and versatile plasma-induced nitrogen doping method was proposed to improved electrical conductivity and even more active sites for Zn nucleation (Fig. 7h)[134]. In addition, other zincopohilic metal nitrides (Cu_3N[135]. and TiN[136].) with high conductivity were constructed on the Zn surface by magnetron sputtering treatment. Especially, by the Cu_3N coating, 2D atom diffusion could be well confined for Zn deposition, achieving entire and uniform Zn nucleation to eliminate bulk dendrite formation[135]. While the TiN protective layer with the (200) orientation can not only effectively

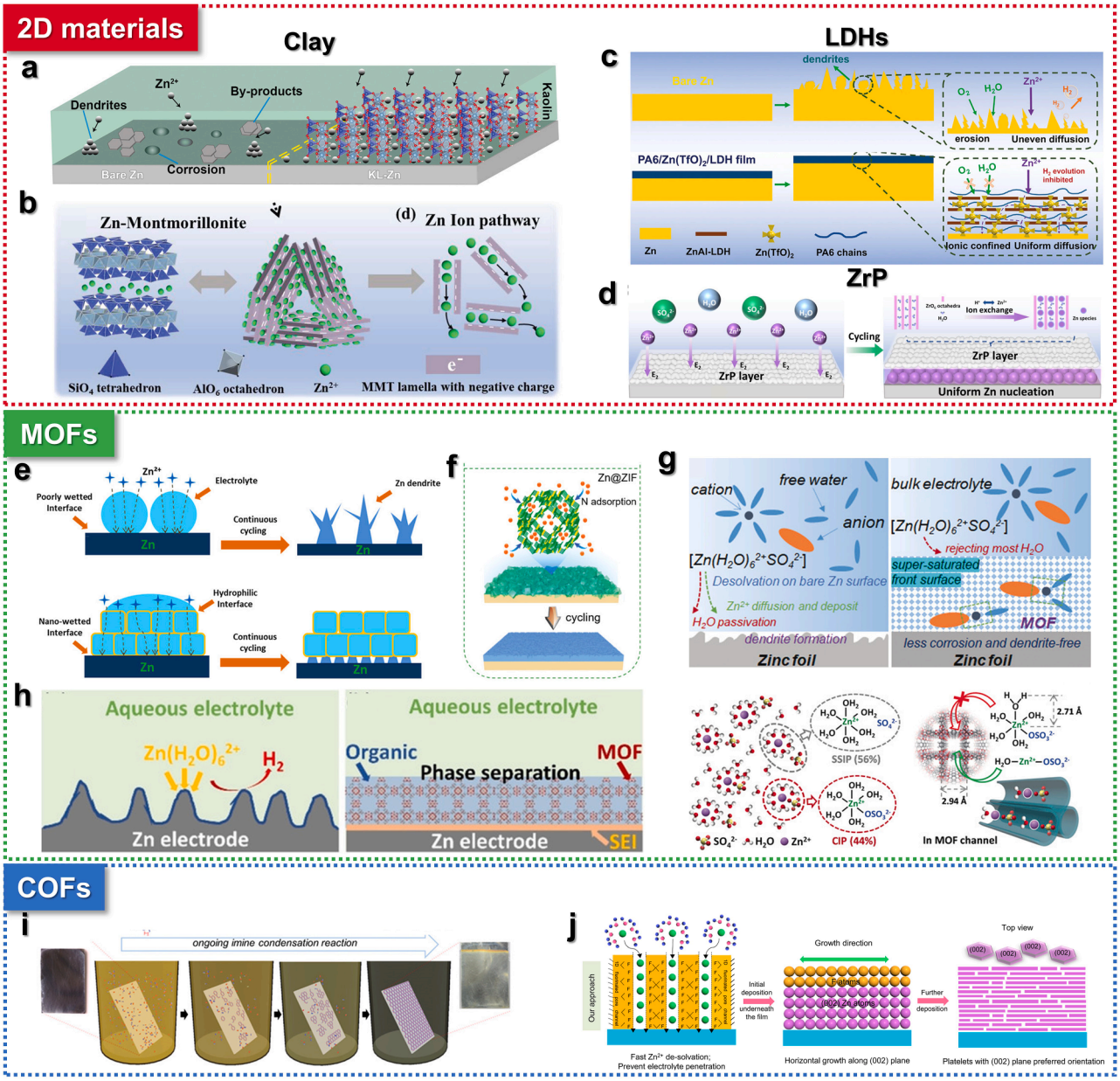

Fig. 8. (a) Schematic illustrations of morphology of Zn and KL-Zn anodes during Zn^{2+} deposition process. Reproduced with permission[138]. Copyright 2020, Wiley-VCH. (b) Crystal structure of Zn-based MMT, magnified Zn-based MMT interface, and charge distribution in MMT lamella. Reproduced with permission[139]. Copyright 2021, Wiley-VCH. (c) Schematic illustration of Zn dendrite growth on different Zn metal anodes. Reproduced with permission[141]. Copyright 2021, Wiley-VCH. (d) The effect of ZrP-based AIL on Zn deposition. Reproduced with permission[143]. Copyright, 2022 Elsevier. (e) Proposed Zn Plating Mechanisms on Bare Zn and MOF–PVDF-Coated Zn. Reproduced with permission.[147]. Copyright 2019, American Chemical Society. (f) The schematic diagrams for Zn@ZIF anode during cycling. Reproduced with permission[148]. Copyright 2020, Wiley-VCH. (g) Upper: schematic illustration of the surface evolution of Zn with/without MOF coating; lower left: two solvation structures in saturated (3.3 m) $ZnSO_4$ aqueous solutions; lower right: schematic illustration of highly coordinated ion complexes of H_2O-Zn^{2+}·OSO_3^{2-} migrating through MOF channels. Reproduced with permission[152]. Copyright 2020, Wiley-VCH. (h) Left: water side reaction and Zn dendrite formation on Zn foil; right: SEI formation in MOF confined organic electrolyte that is immiscible with aqueous electrolyte. Reproduced with permission[157]. Copyright 2020, Wiley-VCH. (i) Scheme illustrating self-assembly of a continuous COF film on a solid substrate. Insets in the leftmost and the rightmost schemes are optical images of, respectively, bare Zn before COF deposition and COF-coated Zn after one day of dip-coating growth. Reproduced with permission[162]. Copyright 2021, Wiley-VCH. (j) Mechanism comparison of the deposition processes for FCOF@Zn surface. Reproduced with permission.[163]. Copyright 2021, Springer Nature.

suppress both the Zn dendritic growth and side reactions but also regulate the growth pattern of the byproduct (Zn hydroxide sulfate) by inducing a lateral growth[136].

Thanks to the unique chemical, physical, and mechanical properties, two-dimensional (2D) materials have been extensively employed as protective coating layers to solve the dendrite problems in Li/Na metal-based battery systems and extended to Zn anodes in aqueous Zn-ion batteries[137]. For instance, Zhou's group employed a sieve-element functional, uniform size porous, and low-cost 2D kaolin to alleviate the issues of metal Zn anode (Fig. 8a)[138]. The kaolin-coated Zn anodes exhibited high self/electrochemical corrosion resistance and dendrite suppression in both symmetrical cells and practical full-cell configuration due to confined Zn^{2+} migration by this layer channel and the existence of abundant adsorption sites such as O−H and Si−O bonds, which can absorb Zn^{2+} and guide the deposition process. After that, another kind of 2D clay named Montmorillonite (MMT) was also developed as an artificial SEI film to alleviate corrosion reactions and inhibit the growth of Zn dendrites.[139, 140] The interlamellar in MMT acts as the freeway for cation transportation, and Zn^{2+} migrates into the interspace of the lamella driven by the electric field (Fig. 8b)[139]. As typical 2D materials, layered double hydroxides (LDHs) are a huge family of ionic lamellar compounds, which are consist of positively charged brucite-like layers with an interlayer space containing solvation molecules and charge compensating anions.[141, 142] The layer structure with appropriate interlayer distance in LDHs serves as ion channels for the facile transport of Zn^{2+}[142]. Shao *et al.* demonstrated an ultrathin heterogeneous interfacial film to stabilize Zn metal anode by coassembling polyamide 6 (PA6), $Zn(TfO)_2$, and LDHs (Fig. 8c)[141]. The 2D interlayer space between PA6 and LDHs achieves the robust confinement of $Zn(TfO)_2$ salt *via* unique hydrogen bond networks in the PA6/$Zn(TfO)_2$/LDH film, which promotes the fast and homogeneous Zn^{2+} diffusion at the electrode interface, giving rise to uniform nucleation and growth of Zn. Moreover, inspired by the exchange property, intercalation chemistry, and anti-corrosion of layered structure $Zr(HPO_4)_2{\cdot}H_2O$ (α-ZrP), Li *et al.* constructed a versatile ZrP-based AIL Zn anode by spray coating technology to promote the electrochemical performance of AZBs (Fig. 8d)[143]. They demonstrated that the ZrP-based AIL provides fast Zn ion transfer channels in the interlayers of ZrP and redistribute the Zn^{2+} ion flux at the interface of Zn anode, therefore promoting the transport of Zn^{2+} ion. Meanwhile, the ZrP-based AIL delivers the merits of high ionic conductivity, improved Zn^{2+} desolvation capability and good wettability. Very recently, n-butylamine was selected to intercalate into monodisperse hexagonal nanoplates of α-ZrP, successfully improving the compatibility with N-methyl pyrrolidone (NMP) and PVDF[144]. The obtained layer on Zn is dense and robust, thus reducing the direct exposure of Zn to electrolytes and well suppressing the side reactions. This intercalation also increases the interlayer spacing and improves the charge transfer, enriching the future selection of conductive inorganics. Additionally, other 2D materials, such as MoS_2[145]. and Zn-$Sb_3P_2O_{14}$[146]. were also proposed to regulate Zn electrodeposition.

Recently, metal-organic frameworks (MOFs) have been used to regulate the diffusion, nucleation, and deposition behaviors of Zn^{2+}. For example, Pan *et al.* built a composite protective layer consisting of nanosized Universistetet I Oslo-66 (UIO-66) to improve the wetting of aqueous electrolytes on the Zn anode (Fig. 8e)[147]. The nanowetting effect of the MOF facilitates an ion flux on the Zn anode to maximize the interface contact between the solid and liquid. Especially, the zeolitic imidazolate framework-based MOFs (ZIF-8,[148–151]. ZIF-7,[152]. and ZIF-11[153]) with a regular porous structure to transfer Zn^{2+} and insulating features to block electrons are regarded as promising artificial SEI-like candidates to modify the Zn anode. The *in situ* grown ZIF-8 layer was used as the ion modulation layer could tune the diffusion behavior of Zn^{2+} on Zn anode (Fig. 8f)[148]. The well-ordered nanochannels and N species of ZIF-8 can effectively homogenize Zn^{2+} flux distribution and modulate the plating/stripping rate, ensuring uniform Zn deposition without dendrite growth. In particular, a super-saturated electrolyte front surface could be accomplished with ZIF-7 (2.94 Å in size window) and ZIF-11 (3.0 Å in outer pore diameter) coating, thereby achieving a homogeneous Zn deposition (Fig. 8g).[152, 153] The porous non-conductive layer positioned onto the Zn surface would regulate the solvation structure prior to receiving charge in the aqueous electrolyte. Consequently, the number of active water molecules that contact the surface of the current collector would be reduced, and the cation concentration at the deposition interface could be increased by self-concentration and electrokinetic coordination mechanism, thereby effectively inhibiting side reactions and dendrite. Very recently, molecular sieves with ordered mesoporous channels are reported to tailor the local electrolyte solvation structure on the Zn surface *via* the same mechanism[154]. Zn^{2+} forms a unique coordination environment through the confinement effect in the optimized channel, and the MCM41-Zn anode showed homogeneous Zn deposition behavior and inhibited side reactions simultaneously. Moreover, another HKUST-1 ($Cu_3(BTC)_2$) MOF has 3D channel structure with highly ordered micropores of ~9 Å, which could confine tris(2,2,2-trifluoroethyl)phosphate (TFEP, <6.6 Å) and Zn^{2+} (0.74 Å) to completely infiltrate into the micropores.[155, 156] Thus, Wang *et al.* coated a ~1.0 μm HKUST layer on Zn and then infiltrated $Zn(TFSI)_2$-TEEP electrolyte into the pores of MOFs to minimize the water content on the Zn surface (Fig. 8h)[157]. The MOF encapsulated $Zn(TFSI)_2$-TFEP forms a ZnF_2-$Zn_3(PO_4)_2$ SEI preventing Zn dendrite and water decomposition. Similar strategies could be applied in the application of $Zn_3(BTC)_2$ layer, which expelled the solvated water molecules and restricted the side reactions[158].

Phytic acid (PA), a natural and low-cost organic molecule extracted from cereals and grains, was chosen as a representative organic linker to build a multifunctional metal-PA complex interphases. Inspired by the PA anticorrosion coating layer for industrial metal protection, a dense and conformal Zn-PA complex layer was formed on the Zn anodes through a feasible, rapid wet-chemistry chelating reaction.[159, 160] The *in situ* formed uniform Zn-PA interlayer allowed a highly zincophilic interface to achieve smooth 3D diffusion, high Zn^{2+} transference number, low polarization resistance, homogeneous interfacial electric field distribution, and reduced desolvation energy of Zn^{2+}, thus kinetically promoting fast and dendrite-free Zn deposition.

Covalent organic frameworks (COFs), a versatile platform with adjustable pore sizes, tailored functional groups, light-weight, and structural stability through covalent bonding, can be used as an alternative to MOFs in the construction of high-performance batteries[161]. Moreover, COFs have functional groups that can provide fast Zn^{2+} transport channels and well-distributed nucleation sites. Grzybowski *et al.* demonstrated the self-assembly of large-area, robust yet flexible (<200 MPa), nanoporous, and ultrathin (20–100 nm) COF films directly on Zn anodes, either planar or curvilinear, which can suppress dendrite growth and formation of electrochemically inactive Zn byproducts, and guide homogeneous Zn deposition (Fig. 8i)[162]. Later, Guo *et al.* developed fluorinated 2D porous covalent organic framework (FCOF) film as a multi-functional platform to protect Zn anode (Fig. 8j)[163]. The strong interaction between fluorine (F) in FCOF and Zn reduces the surface energy of the Zn (002) crystal plane, enabling the preferred growth of (002) planes during the electrodeposition process. Furthermore, the F-containing nanochannels facilitate ion transport and prevent electrolyte penetration for improving corrosion resistance. Very recently, a cation-conducting sulfonic acid-containing COF (TpPa-SO_3H) was applied to coat on the Zn anodes surface[164]. Apart from the advantages discussed above, the sulfonic acid group film can coordinate with Zn^{2+} and decrease the dissolution barrier of Zn^{2+}, forming abundant Zn transport channels and constraining 2D Zn^{2+} diffusion. The detailed ion-coordinated mechanism will be clarified in **3.2.1.2**. To better compare the electrochemical performance of Zn anodes with various ion-guided layers, the interfacial materials, processing method, testing conditions, and electrochemical performances of different materials relevant to artificial interphases are summarized in Table 2.

Table 2
Summary of the battery performances of Zn anodes enhanced by ion-guided layers in symmetric cells.

Artificial interphase	Processing Method	Electrolyte	Current (mA cm^{-2}) @Capacity (mAh cm^{-2})	Lifespan (h)	Thickness of Zn (μm)	Average CE@cycle number	Refs.
$CaCO_3$	Doctor blading	3M $ZnSO_4$+0.1M $MnSO_4$	0.25@0.05	840	–	–	93
TiO_2	ALD	3M $Zn(OTf)_2$	1@1	150	–	–	94
F-TiO_2	Doctor blading	1M $ZnSO_4$	1@1	460	30	–	95
TiO_2-PVDF	Drop cast	2M $ZnSO_4$	0.885@0.885	2000	80	99.4%@1000	96
			8.85@8.85	250	25		
PDMS/TiO_{2-x}	Spin coating	3M $ZnSO_4$	1@1	900	–	99.6%@700	97
			10@10	300			
ZnO-3D	Chemical deposition	2M $ZnSO_4$+0.1M $MnSO_4$	5@1.25	500	100	99.55%@300	98
ZnO HPA	Periodic anodizing	1M $Zn(CF_3SO_3)_2$+0.1M $MnSO_4$	0.2@0.2	1000	100	–	99
			1@1	400			
			5@2.5	100			
Al_2O_3	ALD	3M $Zn(CF_3SO_3)_2$	1@1	500	200	–	100
$ZnMoO_4$	Chemical deposition	3M $ZnSO_4$	0.25@0.125	1000	–	–	101
			1@1	1000			
			10@1	2000			
Oxyhydroxide	Chemical decoration	2M $ZnSO_4$	1@1	4000	250	–	102
			5@5	85			
$BaTiO_3$	Doctor blading	2M $ZnSO_4$	1@1	2000	30	–	103
			5@2.5	1500			
Poled $BaTiO_3$	Doctor blading	1M $ZnSO_4$+0.1M $MnSO_4$	1@1	4100	100	–	104
			10@2	1300			
			20@2	630			
			40@2	158			
$KTa_{1-x}Nb_xO_3$	Doctor blading	1M $ZnSO_4$	1@1	1200	50	97.6%@200	105
			2@1	800			
PVDF	Spin coating	2M $ZnSO_4$	0.25@0.05	2000	–	96.5%@200	106
			1.5@0.3	100			
P(VDF-TrFE)	Spin coating	2M $ZnSO_4$	0.2@0.2	2000	–	–@350	107
ZrO_2	Casted	2M $ZnSO_4$	0.25@0.125	3800	–	99.36%@230	108
			5@1	2100			
Sc_2O_3	Casted	2M $ZnSO_4$+0.1M $MnSO_4$	1@1	200	–	99.85%@260	109
CeO_2	Chemical deposition	2M $ZnSO_4$+0.1M $MnSO_4$	4.4@1.1	1200	–	99.1%@120	110
CeO_2	Scraped	2M $ZnSO_4$	0.5@0.25	1300	80	–@180	111
			5@2.5	1300			
Si_3N_4-PAN	Drop-casted	2M $ZnSO_4$	0.25@0.25	800	30	98.2%@200	112
			1@1	800		98.7@200	
			5@5	400			
			10@10	250			
$NaTi_2(PO_4)_3$	Doctor blading	2M $ZnSO_4$	1@1	260	–	–	113
$Zn_3(PO_4)_2$-Nafion	Drop-casted	1M $ZnSO_4$	0.5@0.25	2800	–	–	114
			2@1	900			
$Zn_xV_2O_5{\cdot}nH_2O$	Chemical decoration	2M $ZnSO_4$	0.25@0.05	560	–	–	115
ZnS	*In situ* vapor-solid strategy	2M $ZnSO_4$	2@2	1100	10	99.2%@200	116
S-MXene@ZnS	*In situ* vapor-solid strategy	2M $ZnSO_4$	0.5@0.5	1600	–	–	117
			1@1	1100			
			5@5	400			
ZnSe	*In situ* vapor-solid strategy	2M $ZnSO_4$	1@1	1500	100	–	118
			10@1	1500			
			10@5	160			
ZnSe	*In situ* vapor-solid strategy	2M $ZnSO_4$	1@1	1530	90	99.2%@400	119
			30@10	172			
ZnSe	Vapor-solid reaction	2M $ZnSO_4$	1@0.5	1700	–	–	120
			2@1	1500			
N/Se-MXene@ZnSe	*In situ* vapor-solid strategy	2M $ZnSO_4$	1@1	2500	–	–	121
			2@1	1500			
			5@5	700			
			10@10	800			
ZnP	Electrodeposition	2M $ZnSO_4$	2@0.5	3300	100	99.5%@200	122
			5@1.25	3200			
			10@2.5	1900			
ZnF_2	Electrodeposition	2M $ZnSO_4$	0.5@1	500	100	99.5%@1000	123
			10@1	500			
			1@1	800			
ZnF_2	High-temperature treatment	2M $ZnSO_4$	1@1	2500	200	99.5%@1000	124
			2@1	2500			
			5@1	2500			
ZnF_2	High-temperature treatment	2M $ZnSO_4$	0.5@0.5	700	30	98.3%@100	125
$ZnF_2/Zn_3(PO_4)_2/CF_X$	Chemical/electrochemical reaction	2M $ZnSO_4$	1@2	500	100	–	126
			14.2@7.1	187			
ZnF_2-Ag	Replacement reaction	2M $ZnSO_4$	2@2	2200	–	99.1%@500	127
ZnF_2-CuZn	Replacement reaction	1M $ZnSO_4$	1@1	2000	50	–	128
			3@3	700			

(*continued on next page*)